Advanced Metrology Suite for Linking Residual Stress to Fundamental Properties of Thermoset Packaging Materials

Polette Centellas
National Intitute of Standards and Technology
Gaithersburg, MD, USA
polette.centellas@nist.gov
ORCID: 0000-0003-3248-3409

Stian Romberg
National Intitute of Standards and Technology
Gaithersburg, MD, USA
stian.romberg@nist.gov
ORCID: 0000-0003-1026-2023

Ran Tao
National Intitute of Standards and Technology
Gaithersburg, MD, USA
ran.tao@nist.gov
ORCID: 0000-0002-5208-7895

Alexander K. Landauer
National Intitute of Standards and Technology
Gaithersburg, MD, USA
alexander.landauer@nist.gov
ORCID: 0000-0003-2863-039X

Karl F. Schoch, Jr.
Materials and Processes, Northrop Grumman
Baltimore, MD, USA
k.eric.schoch@ngc.com

Huong Giang Nguyen
National Intitute of Standards and Technology
Gaithersburg, MD, USA
huong.nguyen@nist.gov
ORCID: 0000-0002-1052-7565

Gale Holmes
National Intitute of Standards and Technology
Gaithersburg, MD, USA
gale.holmes@nist.gov
ORCID: 0000-0002-5639-4112

Gery Stafford
National Intitute of Standards and Technology
Gaithersburg, MD, USA
gery.stafford@nist.gov
ORCID: 0000-0003-3445-9402

Christopher Soles
National Intitute of Standards and Technology
Gaithersburg, MD, USA
christopher.soles@nist.gov
ORCID: 0000-0002-1963-6039

Abstract—**Residual stresses inevitably develop in thermosetting materials used for semiconductor packaging during the curing process and in service. Understanding the development of these deleterious stresses is necessary for improving predictive models and engineering design. Here, we present a suite of metrologies and methodologies, including advanced thermal analysis, rheological characterization, shrinkage, and evolved stress measurements, to link residual stress development with fundamental material properties in a commercial liquid encapsulant.**

Keywords—liquid encapsulant, cure kinetics, rheology, cure shrinkage, residual stress

I. INTRODUCTION

Semiconductor packaging materials are typically thermosetting polymer formulations with multiple components. In these materials, residual stresses develop during the curing process and are closely linked with the reaction kinetics, liquid-to-solid transition, and cure-induced shrinkage [1]. Residual stresses continue to evolve in the cured material in response to hygrothermal conditions during service [2]. Characterizing these behaviors is often challenging due to the complex formulations used in the semiconductor industry. However, understanding the development of residual stresses is necessary to inform predictive models and thus improve the engineering design and manufacturing productivity of semiconductor assemblies.

Here, we present a suite of advanced metrologies and methodologies to measure and analyze the fundamental material properties of a commercial liquid encapsulant. Thermal analysis is used to measure and accurately model the cure kinetics for complex mechanisms. Rheological measurements supplement the cure kinetics study and are used to identify the liquid-to-solid transition during curing. Thin film curvature measurements demonstrate that this transition accurately predicts the development of residual stress caused by the observed cure-induced shrinkage. Stress measurements on the post-cured material further reveal the effect of hygrothermal conditions on the mechanical response. Taken together, this metrology suite ties fundamental to part-scale measurements for a holistic understanding of the evolution of residual stresses during curing and in service, an essential step for improving predictive models.

II. EXPERIMENTAL

A. Chemical Composition

All experiments are performed on a commercial liquid encapsulant designed for semiconductor devices. As shown in **Table I**, the formulation comprises multiple epoxy resins with varying concentrations. It also includes a reactive diluent to reduce the resin viscosity while still participating in the curing process [3], an adhesion promoter to couple organic and inorganic components [4], and inorganic silica fillers to match the coefficient of thermal expansion of the encapsulant with other device components [5]. The latent curing agents inhibit the curing of epoxy resin to prolong the processing time of the

Name (information provided by supplier in safety data sheet)	Description	Mass fraction (%)
Formaldehyde, oligomeric reaction products with 1-chloro-2,3-epoxypropane and phenol	Epoxy resin	21-30
4,4'-isopropylidenediphenol/epichlorohydrin copolymer	Epoxy resin	0-5
p-(2,3-epoxypropoxy)-N,N-bis(2,3-epoxypropyl)aniline	Epoxy resin	0-5
[[(2-ethylhexyl)oxy]methyl]oxirane	Epoxy reactive diluent	0-5
Silane,trimethoxy[3-(oxyranylmethoxy)propyl]-	Epoxy silane adhesion promoter	0-5
Guanidine,cyano-	Amine latent curing agent	0-5
1,3,5-Triazine-2,4,6(1H,3H,5H)-trione, compd. with 6-(2-(2-methyl-1H-imidazol-1-yl)ethyl)-1,3,5-triazine-2,4-diamine (1:1)	Imidazole-based latent curing agent[a]	0-5
Silica	Inorganic filler	61-70
Carbon black	Inorganic filler	0-5

[a.] Compound is comprised of a cyanuric acid component and an imidazole component modified to include primary amine functional groups.

material [6]. The encapsulant is stored in a freezer at -40 °C and allowed to thaw to room temperature before use.

B. Curing Schedule

The stress and strain developed in polymeric materials are dependent on the curing process. Therefore, all samples are cured in air according to the supplier recommendation of 60 min at 100 °C followed by 60 min at 165 °C. Rheological experiments to determine the liquid-to-solid transition are performed at 100 °C for 100 min.

III. METROLOGY SUITE

A. Differential Scanning Calorimetry for Cure Kinetics

Differential scanning calorimetry (DSC) is widely used within the semiconductor community to investigate the cure kinetics of electronic packaging materials [5], [7]–[9]. Prior work by Tao et al. [7] outlines several best practices for DSC measurements on epoxy molding compounds, which we implement to study the liquid encapsulant. All measurements are performed using a DSC equipped with a refrigerated cooling system under nitrogen purge gas. About 10 mg to 15 mg of uncured encapsulant samples are sealed in 40 µL hermetic pans for measurement. The heat flow ($\dot{Q}$) is measured as a function of temperature (T) by heating samples from -40 °C to 300 °C at constant heating rates $\beta = (0.5, 1, 5,$ and $10)$ °C min^{-1}. The standard uncertainties for temperature and heat flow are approximately ± 1 % and ± 3 %, respectively. The degree of cure or conversion as a function of temperature, $\alpha(T) = \int \dot{Q} dT / \beta \Delta H_T$, is calculated by integrating the exothermic reaction peaks starting from a temperature below the onset of the reaction, dividing by the total heat of reaction (ΔH_T), and normalizing by the heating rate. The conversion rate is given by $d\alpha/dt$. To replicate the recommended curing schedule, we perform an isothermal DSC test at 100 °C for 60 min, followed by a second isothermal test at 165 °C for 60 min. Model-based kinetics analysis and simulation are performed using a commercial software following ICTAC recommendations for the analysis of multi-step kinetics [10].

B. Rheometry for Liquid-Solid Transition

Rheometry is a versatile technique for measuring the time-evolving material properties of various materials, including viscoelastic liquid encapsulants. Using a rotational rheometer, we measure the viscoelastic storage (G') and loss (G'') moduli of the uncured encapsulant by deforming a small sample between two 8-mm disposable aluminum parallel plates according to a user-defined oscillating profile of strain amplitude (γ) and angular frequency (ω). The instrument has a minimum resolvable torque of ± 0.05 µN m and angle of ± 0.04 µrad. The storage and loss moduli represent the elastic and dissipative behavior, respectively, and arise due to the stress-strain phase lag inherent to viscoelastic materials. We identify the critical strain below which the viscoelastic moduli are strain-independent, i.e., the linear viscoelastic region [11], by conducting amplitude sweep experiments where γ is varied from 0.1 % strain to 100 % strain at isothermal temperatures up to 100 °C. The critical strain is temperature-dependent, with the lowest value ($\gamma \approx 0.3$ % strain) occurring at 100 °C. Therefore, we maintain the strain amplitude well below this critical value in consecutive experiments to measure the linear viscoelastic moduli.

To investigate the temperature evolution of the moduli during the first heating ramp, we heat a sample from nominally 40 °C to 100 °C at 5 °C min^{-1}, hold at 100 °C for 5 min, then cool back down to 40 °C at 5 °C min^{-1}. As will be further discussed in a later section, the material exhibits rapid gelation kinetics, which makes it difficult to identify the liquid-to-solid transition. Therefore, we use a nascent approach called optimally windowed chirps (OWCh), which involves applying a frequency-varying deformation profile to obtain measurements at significantly faster acquisition times compared to the classical single-frequency method [12]. The OWCh parameters can be designed to apply much lower strain amplitudes than rapid 'multiwave' methods [13], allowing for measurements well below the critical strain. We measure the time evolution of the moduli at 100 °C by continuously applying a modulated deformation profile, where $\gamma << 0.3$ % strain and ω is varied from 0.9 rad s^{-1} to 25.2 rad s^{-1}. The time corresponding to the liquid-to-solid transition is defined when the loss tangent, $\tan\delta = G''/G'$, is independent of frequency [12].

C. Digital Image Correlation for In-situ Strain Measurement

We use a stereo-digital image correlation (DIC) system to measure the strain development in the liquid encapsulant during

433

curing. The system consists of a custom, convective environmental chamber equipped with an antireflective coated viewing window (approximately 300 mm square) and fans to mix air to avoid thermal gradient artifacts (**Fig. 1a**). A pair of 24.4 MPx cameras (exposure time 19 ms) with 50 mm lenses (f/16) is mounted in a custom stereo fixture (stereo angle -18.2°, stand-off 241 mm). The cameras are synchronized and triggered with a data acquisition system. Lighting is provided by three light emitting diode panels with frosted diffusers. Stereo calibration is conducted in the oven volume with the lid removed prior to the experiment. Uncured material (approximately 600 mg to 800 mg) is placed on a thin polyetherimide backer to minimize the effect of boundary conditions and allowed to self-level at room temperature for about 5 min. The sample is black and thus speckled with the minimum necessary matte white spray paint to produce a high-contrast pattern required for DIC analysis. Within about 15 min of speckling, the specimens are cured *in situ* with images collected at 0.5 Hz before and during the recommended curing schedule.

Stereo-DIC analysis is conducted using a commercial software in accordance with the International Digital Image Correlation Society's Good Practices Guide [14]. The analysis parameters are listed in **Table II**. A region of interest (approximately 910 px × 895 px with 1.23 µm px^{-1}) is defined on the flat area of the specimen, avoiding any regions with visually obvious aberrations. The Green-Lagrange Q4 strain fields ($\underline{\epsilon}_{ij_t}$) for each time step are spatially averaged (mean ± standard deviation) and the vector magnitude is computed for each time point. This strain $\left|\underline{\epsilon}_{ij_t}\right|$ is taken to be the bulk strain associated with cure shrinkage convolved with thermal strain. The measurement uncertainty is defined as the geometric sum of the noise floor (22.4 µm m^{-1}) and standard deviation of the strain from the spatial averaging, since the cure shrinkage strain field is nominally homogeneous.

TABLE II.   DIC HARDWARE AND SOFTWARE PARAMETERS

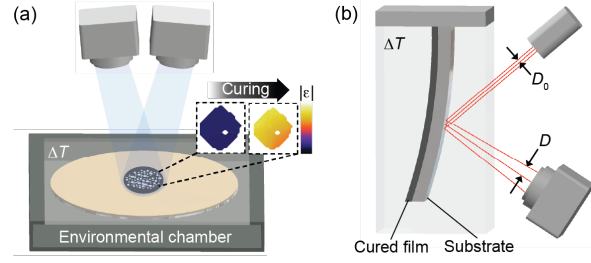| Parameter [unit]	Value
Image filtering	Gaussian 5 px kernel
Reference image	Cumulative with update for iteration > 6
Interpolation	Bi-cubic spline
Matching criterion	Zero-normalized sum-of-square differences with Gaussian weighting
Subset size [px]	41
Step size [px]	19
Subset shape function	Affine
Strain Window	21
Virtual strain gauge [px]	421

Fig. 1 Schematics for test setups. (a) DIC setup using a camera pair focused on the uncured encapsulant to track strains during curing. (b) Setup to measure the curvature of a cured encapsulant film cast on a silicon cantilever using a multi-beam optical stress sensor.

D. Thin Film Curvature for Residual Stress Measurement

We investigate the residual stress in the cured encapsulant in response to varying hygrothermal conditions by measuring the curvature of thin films cast on a cantilever substrate. The sample is prepared by blade-coating a film of the uncured material (78.9 ∝m ± 12.7 ∝m thick) onto a cantilever (4 mm wide × 35 mm long × 583.3 ∝m ± 0.6 ∝m thick) diced from a silicon wafer (100). The coated cantilever is then cured in an oven according to the recommended curing schedule. The cured sample is dried at 65 °C for 48 h under vacuum and then mounted in a 25 mL Pyrex chamber. A digital hygrothermal sensor is placed near the sample to measure the environmental temperature and relative humidity (RH). The sample environment is dried to approximately 2 % RH by flowing dry air into the chamber. Then, a computer-controlled Joule heating element located inside the chamber executes repeated heat-cool cycles by heating to 65 °C, then cooling to 35 °C under reflow of dry air.

The sample curvature is simultaneously monitored using a commercial multi-beam optical stress sensor. The optical sensor generates a 3 × 1 array of laser beams that reflect off the cantilever substrate and into a charge coupled device (CCD) video camera. The curvature is measured by, $\kappa = (D - D_0 / D_0)(\cos\theta / 2L)$, where D is the average spacing between adjacent laser spots in the reflected array, D_0 is the average spacing for a flat substrate ($\kappa = 0$), L is the distance between the cantilever and CCD, and θ is the angle of incidence (**Fig. 1b**). The curvature resolution is typically 2×10^{-4} m^{-1}, or 5 km radius of curvature [15]. The film stress (σ) is calculated from the cantilever curvature using Stoney's formula for an arbitrary thickness and modulus ratio between the film (f) and substrate (s) [16],

$$\sigma = \frac{\kappa\, h_s^2 M_s}{6 h_f A_1}, \quad A_1 = \frac{1+h}{1 + hm(4 + 6h + 4h^2) + h^4 m^2} \quad (1)$$

where $h = h_f / h_s$ is the thickness ratio and $m = M_f / M_s$ is the biaxial elastic modulus ratio. The biaxial elastic modulus, $M = E/(1\text{-}v)$, is a function of Young's modulus (E) and Poisson's ratio (v). The reported elastic properties of the silicon substrate are $E_s = 130$ GPa, $v_s = 0.28$, and $M_s = 181$ GPa [15];

the assumed properties of the encapsulant film are $E_f = 3.99$ GPa [17], $v_f = 0.35$, and $M_f = 6.14$ GPa. The stress resolution corresponding to the curvature resolution is approximately 0.02 MPa.

For a material undergoing elastic deformation, the stress is related to strain according to Hooke's law, $\sigma = M\,\varepsilon$. The elastic strain developed in the film as the cantilever is thermally cycled is $\varepsilon = (\alpha_s - \alpha_f)\,\Delta T$, where α_s and α_f are the coefficients of thermal expansion of the silicon substrate and encapsulant film, respectively, and ΔT is the temperature change [15]. Taken together, the relationship between film stress and temperature is given by, $\sigma = M_f(\alpha_s - \alpha_f)\,\Delta T$.

Similar film curvature measurements are performed by industry collaborators using a polished 100-mm silicon wafer, spin-coated with the uncured encapsulant (approximately 30 ∝m thickness). The wafer curvature is measured as the encapsulant cures, then as the cured sample is cooled to 25 °C, and finally as the cured sample is heat-cooled between 25 °C and 150 °C for three cycles. This sample is left under ambient conditions for one month, then the wafer curvature is remeasured as the sample is heat-cooled between 25 °C to 200 °C for two cycles. The film stress is calculated from the wafer curvature using Stoney's formula (**Eq. 1**).

E. Water Sorption-Desorption Measurements

Isothermal mass changes in a cured encapsulant sample due to water vapor sorption or desorption at set % RH are measured using an automated vapor sorption analyzer at ambient pressure and with nitrogen (99.999 % purity) as the carrier gas. The desired % RH is obtained by continuously mixing a dry nitrogen flow with a humid nitrogen flow. The instrument has a ± 0.1 μg mass resolution and a ± 1 % RH control standard uncertainty based on manufacturer specifications. A sample with an initial mass of approximately 21 mg is first conditioned for 360 min at 65 °C under pure nitrogen flow (0 % RH). For sorption experiments, the sample environment is then set to 60 % RH for approximately 630 min at an isothermal temperature (25 °C and 50 °C). Then, the sample environment is set to 2 % RH for approximately 360 min at the same isothermal temperature to investigate the desorption behavior. Mass changes during the sorption-desorption experiments are calculated relative to the dry mass measured at the end of the conditioning stage.

IV. RESULTS AND DISCUSSION

A. Measurement and Modeling of Complex Cure Kinetics

The DSC heat flow responses at different heating rates, $\beta = (0.5, 1, 5, \text{and } 10)$ °C min^{-1}, reveal the complex, multi-step cure kinetics of the uncured encapsulant. At higher heating rates, the reaction curves shift to higher temperatures, but the shapes of the exotherms are consistent, indicating that the material undergoes a similar reaction mechanism across all rates tested (data not shown for brevity). **Fig. 2a** shows the calculated conversion rate for the $\beta = 10$ °C min^{-1} measurement. The results indicate that at an onset temperature near 130 °C, a primary curing reaction peak gradually

increases, develops two narrow shoulders, and crests at around 160 °C. The conversion rate then decelerates, and the primary reaction completes at approximately 200 °C. The shape/behavior of the convoluted exotherm highlights the complexity of the curing kinetics of multi-component formulations (**Table I**). Following the primary reaction peak, a second broader reaction peak emerges and tails off around 300 °C. Based on the peak characteristics, we fit the experimental data for all four tested heating rates using a four-step reaction model by optimizing the fit to the heat flow signal (best fits for each step and the overall fit are shown in **Fig. 2a**). The model fit closely matches the experimental data across the entire temperature range with $R^2 = 0.9994$.

The materials data sheet provided by the supplier suggests that these curing reactions are initiated by the thermal activation of one or both latent curing agents in the encapsulant composition, i.e., the amine- and/or imidazole-based agent(s) (**Table I**). Since the amine latent curing agent reacts with epoxy at elevated temperatures around 180 °C [18], we assume that the convoluted reaction observed between 130 °C and 200 °C likely arises from the thermal activation of the imidazole-based latent curing agent. This imidazole-based compound contains
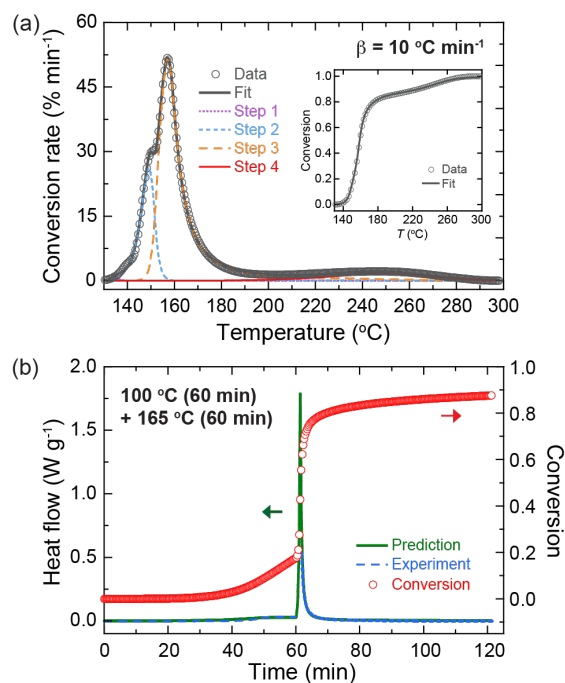
Fig. 2 DSC measurements and cure kinetics modeling. (a) The conversion rate calculated from the heat flow response for $\beta = 10$ °C min^{-1}. The inset shows the conversion curve for the same data. The open circles represent experimental data and the lines are fits to a four-step reaction model ($R^2 = 0.9994$ for the overall fit). (b) DSC heat flow responses (left y-axis) and conversion (right y-axis) during the recommended curing schedule. The experimental measurements and model prediction of the heat flow response are represented by the dashed blue lines and solid green line, respectively. The red open circles represent the predicted conversion.

active hydrogens that readily react with epoxy at moderate temperatures around 75 °C; however, this reaction is relatively slow [19]. At elevated temperatures of around 110 °C, the compound dissociates and frees an imidazole, which autocatalyzes the reaction with epoxy. This reaction proceeds rapidly and completes within minutes [20]. Therefore, the onset of the convoluted reaction peak can be attributed to low-temperature, slow epoxy curing with active hydrogens. The higher-temperature apex can be attributed to an imidazole-catalyzed, self-accelerating epoxy reaction. The conversion curve (**Fig. 2a** inset) shows that rapid conversion to approximately 80 % occurs near the sharp apex, suggesting that the convoluted primary reaction peak is dominated by the imidazole-catalyzed reaction.

We next investigate the cure behavior of the encapsulant during the recommended curing schedule. **Fig. 2b** shows the experimental data and four-step reaction model prediction of heat flow as a function of time. The measured results indicate a small amount of heat generated during the first isothermal dwell at 100 °C, implying limited reaction activity. The bulk of the reaction occurs during the temperature ramp to 165 °C, as observed by the sharp exothermic peak starting around 60 min. Using the reaction model, we also predict the degree of conversion during the curing process (**Fig. 2b**). The predicted conversion profile shows that the reaction onset occurs after 30 min, and achieves under 20 % conversion by the end of the first dwell at 100 °C. By the end of the second dwell at 165 °C, the conversion levels off at approximately 87 %, indicating a slow reaction beyond this point caused by additional reactions of the imidazole-based curing agent [20].

B. Liquid-to-Solid Transition Governs Effective Cure Shrinkage

Rheological measurements on the uncured liquid encapsulant elucidate the temperature evolution of material properties and supplement the DSC measurements. **Fig. 3** shows how the viscoelastic moduli change as the material is slowly heated to 100 °C and then cooled back to 40 °C. At the start of the experiment, the uncured encapsulant is a liquid with $G' < G''$. During the heating ramp, G' crosses G'', which suggests the onset of a curing reaction. G' remains greater than G'' upon cooling, indicating that the modulus crossover was due to an irreversible chemical process during heating. The irreversibility of the crossover is also illustrated by the appearance of a slightly more solid-like sample at the end of the experiment compared to the start (see inset images in **Fig. 3**). This modulus crossover, observed at approximately 85 °C, is likely caused by a chemical reaction between active hydrogens and epoxy, which occurs at moderate temperatures around 75 °C [19], [20]. In contrast, our DSC measurement (at a comparable heating rate of $\beta = 5$ °C min^{-1}) shows that the onset of the first exothermic peak corresponding to the active hydrogen reaction pathway does not occur until at least 120 °C. Since the encapsulant is highly filled with chemically inert silica particles, it is possible that the heat released by a small amount of reactive material is below the DSC sensitivity and thus not resolved in measurements. This also suggests that only
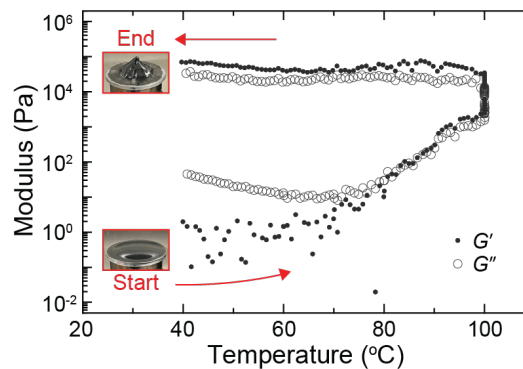

Fig. 3 Temperature-evolution of G' and G'' in the uncured encapsulant during the first temperature ramp to 100 °C. The insets show optical images of the uncured encapsulant at the start and end of the test. The uncertainty of each measurement is at most ± 7 %, except between 70 °C and 80 °C where G'' reaches a minimum and uncertainty is at most ± 20 %, which is small compared to the exponential growth of the moduli.

partial curing occurs upon heating to 100 °C, implying that the sample has formed a weak network of particle contacts and chemical crosslinks that is not strong enough to support residual stress.

The encapsulant will begin to accumulate residual stress when it transitions to solid-like behavior by forming a network of crosslinks that does not depend on easily broken particle contacts [12]. However, the traditional criterion of using the G'-G'' crossover to identify the liquid-to-solid transition cannot be applied to this material since G' surpasses G'' during the ramp to 100 °C (**Fig. 3**). Instead, we use OWCh measurements to identify the transition by determining when the loss tangent becomes independent of frequency [12]. **Fig. 4a** presents the evolving frequency-dependent loss tangent of an uncured sample held at 100 °C. We observe that the liquid-to-solid transition occurs after 60 min, suggesting that the material does not solidify during the first isothermal dwell in the curing schedule. Therefore, we expect residual stress to evolve only during the second isothermal dwell at 165 °C.

From DIC measurements, we find that residual strains begin to accumulate in the uncured encapsulant at two stages: during the first isothermal dwell at 100 °C and around the liquid-to-solid transition identified by OWCh measurements (**Fig. 4b**). Two competing mechanisms for residual strain development in curing thermosets are thermal expansion and volumetric shrinkage due to chemical crosslinking, i.e., cure shrinkage. Using the reported α_f of the cured material, we predict around 0.1 % strain due to thermal expansion during the 100 °C dwell. However, DIC measurements indicate a total strain magnitude well above 0.1 % strain after 10 min into the isothermal dwell, indicating that the dominant mechanism for strain development is cure shrinkage. This observation agrees with our DSC cure kinetics model, which predicts conversion during the 100 °C dwell (**Fig. 2b**). DIC measurements further reveal that cure shrinkage increases during the ramp to and initial dwell at 165 °C, which correlates well with the DSC model prediction
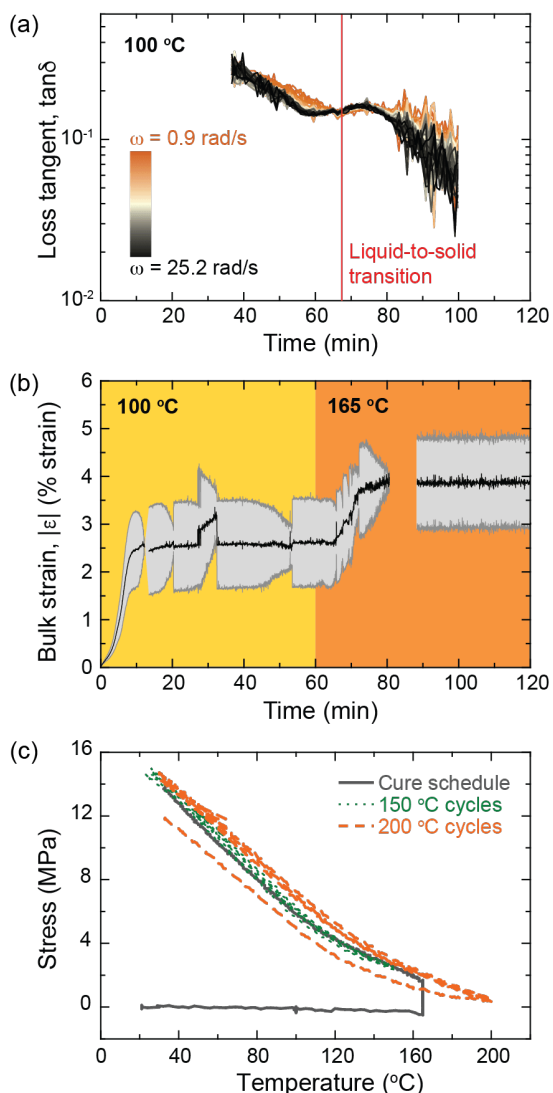
(a)

(b)

(c)

Fig. 4 Time-evolution of material properties in the uncured encapsulant. (a) The loss tangent is measured at 100 °C. The liquid-to-solid transition is indicated by the solid red line. OWCh measurements were directly compared to slower traditional frequency sweeps using a non-curing, but rheologically similar, resin (i.e., with $G' > G''$), which revealed an error of approximately ± 10 % for OWCh measurements. (b) The Green-Lagrange strain magnitude is measured during curing. The yellow and orange regions indicate the isothermal dwells at nominally 100 °C and 165 °C, respectively. Gaps exists where extensive decorrelation occurred. The shaded gray area represents the expanded uncertainty about the mean strain value. (c) Stress measurements are performed on a thin-film coated wafer during the curing process (grey solid line), post-cure thermal cycling to 150 °C (dotted green line), and post-cure thermal cycling to 200 °C (dashed orange line).

of rapid conversion during this temperature transition (**Fig. 2b**) as well as the OWCh identification of the liquid-to-solid transition at approximately 67 min (**Fig. 4a**). At the end of the 165 °C dwell, we measure a stable cure shrinkage of about

4 % strain. Any accumulated strain in the material beyond the liquid-to-solid transition develops residual stress and is referred to as the "effective cure shrinkage" [1]. As expected, *in situ* thin film curvature measurements show that the encapsulant begins to accumulate residual stress around the isothermal dwell at 165 °C (**Fig. 4c**). Therefore, the effective cure shrinkage of the encapsulant is roughly 2 % strain.

C. Residual Stress Under Hygrothermal Conditions

Finally, we investigate the mechanical response of the cured encapsulant film cast on a silicon substrate to changing hygrothermal conditions. The cantilever sample initially bows away from the optical sensor (as depicted in **Fig. 1b**), indicating a tensile stress state in the film arising from both effective cure shrinkage and thermal contraction caused by cooling to room temperature. **Fig. 5a** presents the measured film curvature over 10 heat-cool cycles and reveals a reproducible response, indicating that the film behaves elastically over the test duration [15]. The magnitude of the tensile stress decreases during the heating intervals due to the α mismatch between the encapsulant film ($\alpha_f = 15 \times 10^{-6}$ K^{-1}, value reported in the materials data sheet) and silicon substrate ($\alpha_s = 2.6 \times 10^{-6}$ K^{-1} [15]). In other words, the thermal expansion of the film is constrained by the substrate, which develops a compressive stress that relieves some of the tensile stress in the film.

After the first thermal cycling test, the sample was left in the setup for 5 days under ambient conditions before rerunning the experiment. The curvature measured at the start of this second test is less than the initial curvature of the dried case (indicated by the dashed red line in **Fig. 5b**). The film curvature, and thus the tensile film stress, accumulates in the unconditioned sample over 14 heat-cool cycles and eventually approaches the response measured in the dried test. Two mechanisms that could influence the film stress are residual curing and water uptake. Our DSC heat flow measurement on the cured encapsulant does not show residual curing below 150 °C. Furthermore, any residual curing will further the volumetric shrinkage of the material and thus increase the magnitude of the curvature/stress [1], which contradicts the behavior observed in **Fig. 5b**. Conversely, water vapor sorption studies on silica-filled polymers demonstrate that water uptake causes volumetric expansion and relieves the residual stress developed during curing [2]. To confirm if our cured encapsulant film can uptake water under the test conditions, we perform isothermal water vapor sorption-desorption experiments (**Fig. 5c**). After 630 min at ambient conditions (25 °C, 60 % RH), the sample exhibits about 0.10 % mass gain due to water uptake and did not reach saturation. Therefore, our sample likely continues to uptake water in the 5 days between experiments, in agreement with results on similar encapsulants which achieve saturation at 1.2 % mass gain under the same ambient conditions [22]. Water desorbs quickly upon reducing humidity, with faster kinetics at elevated temperatures. The cured encapsulant exhibits around 0.05 % mass loss at 25 °C and 0.10 % at 50 °C over 360 min, i.e., the duration of the thermal cycling experiment. We propose that moisture is driven from the encapsulant film during thermal cycling, which causes
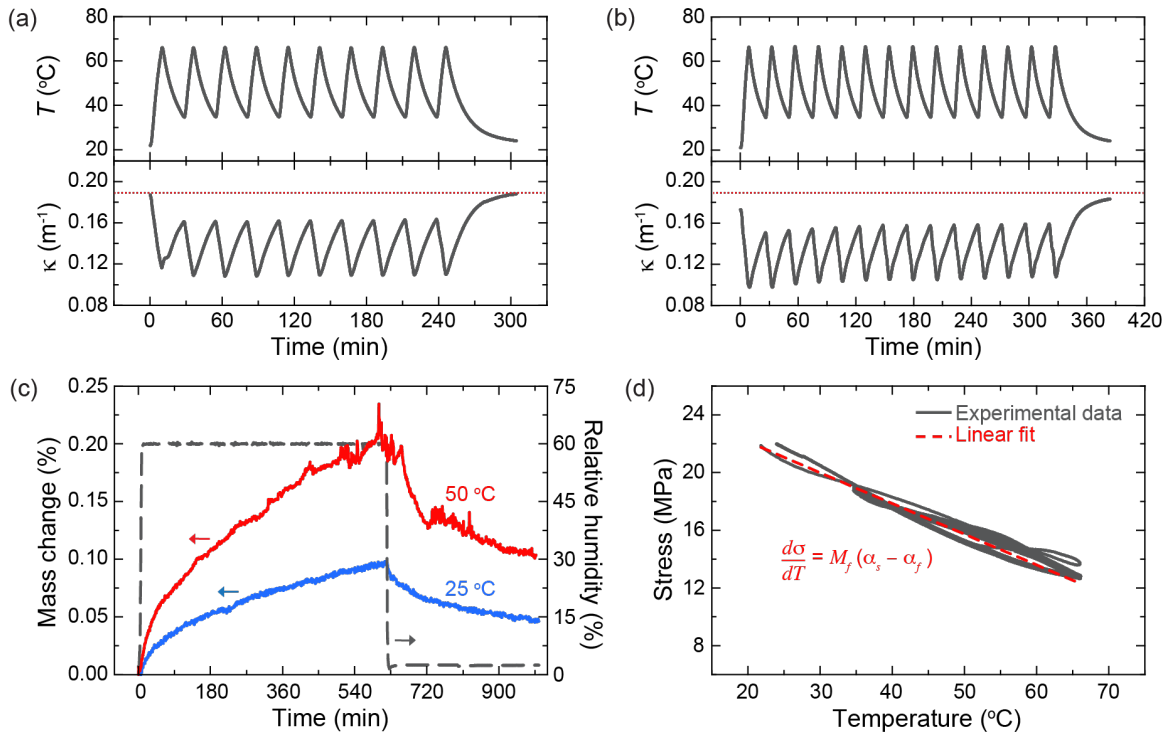
Fig. 5 Hygrothermal effects on the cured encapsulant. Temperature (T) cycling experiments to measure the thin film cantilever curvature (κ) of (a) the sample dried at 65 °C for 48 h and (b) the same sample after 5 days under ambient conditions. The dashed red line indicates the room temperature curvature measured for the dried sample. (c) Isothermal mass changes in a cured encapsulant sample due to water vapor sorption (at 60 % RH), followed by desorption (at 2 % RH) at 25 °C (blue) and 50 °C (red). (d) Calculated film stress from curvature measurements corresponding to the dried sample in (a). The dashed red line is the overall linear fit to the thermal cycling data (R = 0.98).

the film curvature/stress to approach the state measured in the dried sample.

The dried film curvature is replotted as a function of calculated film stress (**Eq. 1**) versus temperature (**Fig. 5d**). From the slope of the linear fit to the experimental data, we extract $\alpha_f = 37 \times 10^{-6}$ K^{-1}. Differences between extracted and reported values can be attributed to the assumed elastic properties used to calculate the film stress and uncertainty associated with measured film thickness. The complementary stress measurements on a film-coated wafer sample support our results (**Fig. 4c**). The calculated stress of the cured film at room temperature is approximately 14 MPa, which is comparable to the value obtained from our cantilever curvature measurements (approximately 22 MPa). The cured film-coated wafer also exhibits a highly repeatable, elastic response over the first set of heat-cool cycles from 25 °C to 150 °C. Much like our cantilever experiments, the wafer sample measures a smaller stress after an extended period at ambient (likely humid) conditions, before recovering its repeatable, elastic response in consecutive thermal cycles (shown in the second set of heat-cool cycles from 25 °C to 200 °C). This finding further suggests that expansion caused by water uptake measurably affects residual stress.

V. CONCLUSION

Through a comprehensive suite of metrology tools, this study establishes a direct link between residual stress evolution and fundamental material chemistry in thermosetting encapsulants. Our DSC experiments reveal a complex, multi-step cure reaction with distinct contributions from different curing agents. Rheometry data identify the liquid-to-solid transition as a key threshold, beyond which accumulated shrinkage strains contribute to long-term residual stress. DIC measurements confirm that processing strains emerge at two critical stages—during the early curing phase and at the liquid-to-solid transition—highlighting the interplay between thermal expansion and cure shrinkage. Thin-film curvature analysis further quantifies residual stress under varying hygrothermal conditions, revealing that moisture uptake can relieve stress over time.

These findings underscore the necessity of advanced characterization techniques to capture the nuanced stress development in highly filled thermosetting materials that occurs both during processing (due to cure shrinkage and solidification) and in service (due to thermal expansion and moisture uptake). The ability to quantify and model stress evolution under processing-relevant conditions is critical for optimizing semiconductor package reliability. Our results not only validate the effectiveness of predictive stress models but

also provide experimental benchmarks for refining material selection and processing strategies.

Looking ahead, integrating molecular-scale investigations with these metrology techniques will deepen our understanding of stress mechanisms in thermosetting polymers. Future efforts will focus on refining measurement accuracy, expanding characterization to additional material formulations, and developing real-time monitoring tools for in-line manufacturing applications. By bridging fundamental materials science with practical engineering challenges, this research paves the way for more reliable and manufacturable semiconductor packaging technologies.

DATA AVAILABILITY

DISCLAIMER

Certain equipment, instruments, software, or materials are identified in this paper to specify the experimental procedure adequately. Such identification is not intended to imply recommendation or endorsement of any product or service by NIST, nor is it intended to imply that the materials or equipment identified are necessarily the best available for the purpose.

ACKNOWLEDGMENT

REFERENCES

[1] S. P. Phansalkar, C. Kim, B. Han and P. J. Gromala, "Volumetic effective cure shrinkage measurement of dual curable adhesives by fiber Bragg grating sensor," *J. Mater. Sci.,* vol. 55, pp. 9655-9664, 2020.

[2] Y. J. Feilzer, A. J. Feilzer, M. J. Noack and C. J. Kleverlaan, "Release of contraction stress of dental resin composites by water sorption," *Dent. Mater.,* vol. 40, pp. 1697-1701, 2024.

[3] A. R. Japtap and A. More, "Developments in reactive diluents: A review," *Polym. Bull.,* vol. 79, pp. 5667-5708, 2021.

[4] J. C. Hoepfner and S. H. Pezzin, "Functionalization of carbon nanotubes with (3-glycidyloxypropyl)trimethoxysilane: Effect of wrapping on epoxy matrix nanocomposites," *J. Appl. Polym. Sci,* vol. 133, pp. 1-10, 2016.

[5] Y. He, B. E. Moreira, A. Overson, S. H. Nakamura, C. Bider and J. F. Briscoe, "Thermal characterization of an epoxy-based underfill material for flip chip packaging," *Thermochim. Acta,* Vols. 357-358, pp. 1-8, 2000.

[6] N. Sawa, T. Nomoto, K. Iuchi, T. Suzuki and S. Kawata, "Imidazole-isocyanuric acid adducts". U.S. Patent 4189577, 19 Feb. 1980.

[7] R. Tao, S. P. Phansalkar, A. M. Forester and B. Han, "Investigation of cure kinetics of advanced epoxy molding compound using dynamic heating scan: An overlooked second reaction," in *2023 IEEE 73rd Electronic Components and Technology Conference (ECTC)*, Orlando, FL, 2023.

[8] S. Shi, T. Yamashita and C. P. Wong, "Development and Characterization of Imidazole Derivative Cured Bisphenol A Epoxy

Materials for Flip-Chip Underfill Applications," in *1999 International Symposium on Advanced on Packaging Materials*, Braselton, GA, 1999.

[9] S.-J. Park, M.-K. Seo and J.-R. Lee, "Isothermal cure kinetics of epoxy/phenol-novolac resin blend system initiated by cationic latent thermal catalyst," *J. Polym. Sci. Part A: Polym. Chem.,* vol. 38, pp. 2945-2956, 2000.

[10] S. Vyazovkin, A. K. Burnham, L. Favergeon, N. Koga, E. Moukhina, L. A. Pérez-Maqueda and N. Sbirrazzuoli, "ICTAC Kinetics Committee recommendations for analysis of multi-step kinetics," *Thermochim. Acta,* vol. 689, 2020.

[11] M. M. Ak and S. Gunasekaran, "Linear viscoelastic methods," in *Nondestructive food evaluation: Techniques to analyze properties and quality*, NY, CRC press, 2000, pp. 287-334.

[12] M. Geri, B. Keshavarz, T. Divoux, C. Clasen, D. J. Curtis and G. H. McKinley, "Time-resolved mechanical spectroscopy of soft materials via optimally windowed chirps," *Phys. Rev. X,* vol. 8, pp. 1-9, 2018.

[13] E. E. Holly, S. K. Venkataraman, F. Chambon and H. H. Winter, "Fourier transform mechanical spectroscopy of viscoelastic materials with transient structure," *J. Non-Newtonian Fluid Mech.,* vol. 27, pp. 17-26, 1988.

[14] E. M. C. Jones and M. A. Iadicola, *A Good Practices Guide for Digital Image Correlation,* International Digital Image Correlation Society, 2018.

[15] J. J. Kim, G. R. Stafford, C. Beauchamp and S. A. Kim, "Development of a dental implantable temperature sensor for real-time diagnosis of infectious disease," *Sensors,* vol. 20, pp. 1-18, 2020.

[16] L. B. Freund, J. A. Floro and E. Chason, "Extensions of the Stoney formula for substrate curvature to configurations with thin substrates and large deformations," *Appl. Phys. Lett.,* vol. 74, pp. 1987-1989, 1999.

[17] P. Dittanet, R. A. Pearson and P. Kongkachuichay, "Thermo-mechanical behaviors and moisture absorption of silica nanoparticle reinforcement in epoxy resins," *Int. J. Adhes. Adhes.,* vol. 78, pp. 74-82, 2017.

[18] T. Güthner and B. Hammer, "Curing of epoxy resins with dicyandiamide and urones," *J. Appl. Polym. Sci,* vol. 50, pp. 1453-1459, 1993.

[19] D. W. Schiering and J. E. Katon, "An infrared spectroscopic investigation of the curing reactions of the EPON 828/meta-phenylenediamine system," *J. Appl. Polym. Sci.,* vol. 34, pp. 2367-2375, 1987.

[20] L. Liu and M. Li, "Curing mechanisms and kinetic analysis of DGEBA cured with a novel imidazole derivative curing agent using DSC techniques," *J. Appl. Polym. Sci,* vol. 117, pp. 3220-3227, 2010.

[21] S. K. Romberg and A. P. Kotula, "Simultaneous rheology and cure kinetics dictate thermal post-curing of thermoset composite resins for material extrusion," *Addit. Manuf.,* vol. 71, pp. 1-13, 2023.

[22] Y. He and Z. Alam, "Moisture absorption and diffusion in an underfill encapsulant at T>Tg and T<Tg," *J. Therm. Anal. Calorim.,* vol. 113, pp. 461-466, 2013.

[23] P. Centellas, S. Romberg, G. Stafford, Schoch, K. F., H. G. Nguyen, R. Tao and A. K. Landauer, "Data for Advanced Metrology Suite for Linking Residual Stress to Fundamental Properties of Thermoset Packaging Materials," National Institute of Standards and Technology, 2025, doi: 10.18434/mds2-3698.